MUSIC-Based Breathing Rate Monitoring Using Wi-Fi CSI

Pin-Jen Lai[1], Yu-Shun Zhan[2], Wei-Lien Yeh[3], Meng-Lin Ku[4], Chih-Min Yu[5]

Department of Communication Engineering, National Central University, Taiwan[1-4]
College of Artificial Intelligence, Yango University, China[5]

Email: jennylai891123@gmail.com[1], abc9041512@gmail.com[2], yehwilliam900701@gmail.com[3], mlku@ce.ncu.edu.tw[4], hankycm7@gmail.com[5]

***Abstract*—Since channel state information (CSI) data can be utilized to sense the subtle changes in the environment, such as chest movement, we provide the analysis of CSI amplitude and phase as a basis for estimating breathing rates. In this paper, a breathing rate monitoring system is proposed, in which CSI data is collected with Intel Wi-Fi Link 5300 wireless network interface card (NIC) and Linux 802.11n CSI Tool [1]. To this end, an antenna and subcarrier selection method is proposed to select those CSIs which are sensitive to respiratory thoracic changes. Furthermore, multiple signal classification (MUSIC) is applied as our research method in the estimation of breathing rates. Extensive experiments are conducted to validate the effectiveness of the proposed system. Our experimental results demonstrate that the proposed system can not only effectively distinguish the breathing state differences of fast, slow, and apnea but also achieve a certain accuracy in the calculation of the breathing rates.**

***Index Terms*- Breathing rate, Wi-Fi, channel state information, multiple signal classification**

I. INTRODUCTION

In recent years, the issue of health detection has attracted more and more attention. The detection of respiration can be used as an important way for vital sign monitoring, but most commercial devices have the disadvantages of high price and inconvenience to wear, or it can only be used to monitor the heart rate. As an alternative, the channel state information (CSI) through wireless signals has been investigated due to its advantages of low cost, wear-free and privacy.

The CSI demonstrates the attenuation factors of the signal on each channel path, such as signal scattering, environmental reflection, distance attenuation and other information. In orthogonal frequency division multiplexing (OFDM) systems, the CSI consists of both subcarrier-level amplitude and phase information. We can extract 802.11n channel information with Intel Wi-Fi Link 5300 wireless NIC and Linux 802.11n CSI Tool [1], which consists of channel frequency response (CFR) samples for 30 OFDM subcarriers.

The CSI can be regarded as an upgraded version of the received signal strength indication (RSSI), and it can be obtained in forms of amplitudes and phases of multipaths on Wi-Fi devices. As compared with the RSSI, the CSI has a certain degree of resolutions in multipath propagation and can detect weak signal fluctuations, thereby improving sensing sensitivity, expanding sensing area and enhancing sensing reliability. The paper [2] discussed methods to extract CSI phases. The idea lies in that the CSI phase and respiration signal are periodic signals with the same frequency, and the measured phases of a given subcarrier from an antenna pair have the same packet detection delay, sampling period, and frequency difference. While the wireless signal is reflected from a person's chest at the breathing frequency, the true phase of the reflected signal at any antenna of the receiver is also periodic with the same frequency. In [3], [4] and [5], a system was proposed for calculating the breathing rate, which also considered the influence of different sleeping postures. The methods such as discrete wavelet transform, outliers removing and filtering are used in the CSI data preprocessing. In [6], a Fresnel zone model was established for Wi-Fi based wireless sensing, and the relationship between human motion and received signals was studied. When an object moves across a series of Fresnel zones, the received signal is a continuous sinusoidal-like waveform. The human respiration resulting in a minute chest movement may only cause the reflection path length to change less than one wavelength, and the received signal is just a fragment of the sinusoidal-like waveform. The authors in [6] also proposed the orthogonality and complementarity of the CSI amplitude and phase. Thus, the system for the respiration detection is mainly through compensating the CSI amplitude with the CSI phase via commodity Wi-Fi to eliminate the blind spots of Fresnel zones. Nonetheless, the aforementioned works [2]-[6] only mentioned the phase analysis or fast Fourier transform (FFT) [7] in the breathing rate estimation. Considering the CSIs are sensitive to noise, in this paper, we aim at applying a multiple signal classification algorithm (MUSIC) for effective noise suppression [8].

In this paper, we detect the breathing rate by utilizing the collected CSI amplitude and phase information. First, the phase calibration and the antenna selection are proposed in the data preprocessing. By comparing the CSI amplitude changes of different subcarriers, we can distinguish which subcarriers are more sensitive to environmental changes. In addition, the CSI phase is more likely to sense the life characteristics of people than the CSI amplitude. When the wireless signals are reflected from the human chest cavity, the CSI phase change can dynamically response to the change in thoracic rise and fall due to the Doppler effect. Next, the phase is unwrapped and denoised by linear transformation, and then the respiration rate is estimated through FFT and refined by the MUSIC.

As compared with commercial wearable or image-based detection devices, the proposed method in this paper is more convenient and can ensure the privacy of users. In addition to the function of real-time observation of measurement data, it is also used with APP to play music that can match the

situation under different breathing rates. Taking an example, when a baby is crying, his respiration rate is a little faster than the normal case, and the system can detect a higher breathing rate and automatically play soft music that can soothe his mood.

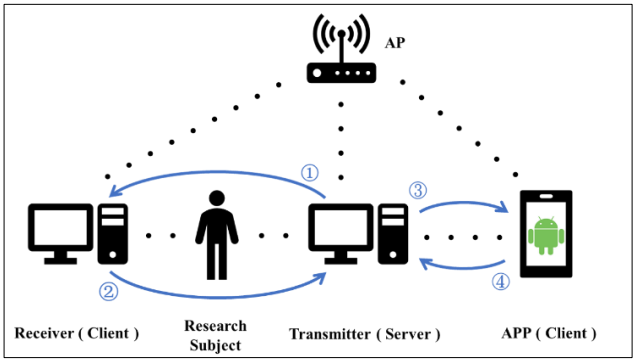

Fig. 1 The architecture and workflow of the proposed breathing rate monitoring system.

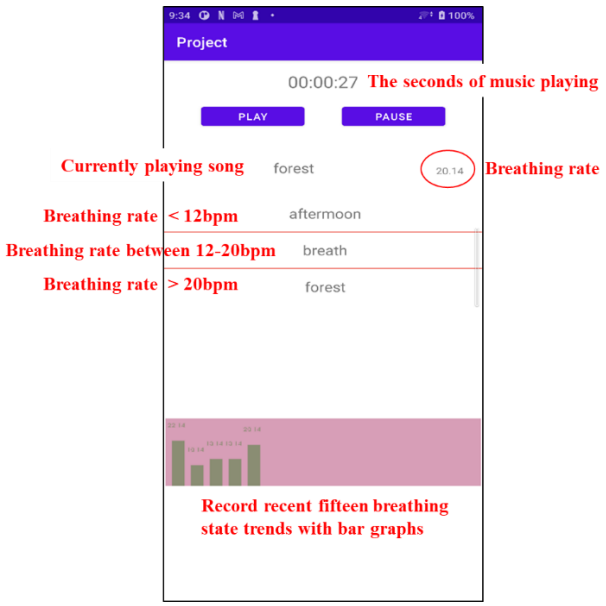

Fig. 2 The APP interface of the proposed system.

II. Proposed System Architecture

The architecture of the proposed breathing rate monitoring system is shown in Fig. 1, consisting of two desktop computers both with an Intel Wi-Fi Link 5300 wireless network interface card (NIC) and three antennas, an access pint (AP), and a phone. At first, we install Linux 802.11n CSI Tool in the Ubuntu 16.04 LTS system, set the environment, and use two hosts, one as the transmitter and the other as the receiver to drive the Intel 5300 NIC. Both the transmitter and the receiver switch the NIC into a monitor mode, and we set parameters, e.g., the sending rate, the number of antennas, and the high throughput mode. In the first phase (Fig. 1 ①)), the transmitter sends packets to the receiver, and at the same time, run "realtime_csi_music.m" through MATLAB to make TCP connection as a server and wait for the client to return data. In the second phase (Fig. 1 ②)), the receiver receives the packets and completes the connection to return data. The real-time CSI visualization can be achieved. The CSI amplitude graph can be observed on the transmitter screen with the changes of wireless environments. In this paper, we set the packet transmission rate 10 Hz, and the transmitter conducts the breathing rate estimation every minute.

In addition to real-time visualization, we also combine computer host with mobile APP to systematize the whole equipment. In the third phase (Fig. 1 ③), the transmitter host is used as the server, and the mobile APP is used as the client. At the same time, the transmitter host and the mobile APP are connected to the same network domain. In the fourth phase (Fig. 1 ④), after the connection is established, the server can transmit the breathing rate value read in the XML file to the client, and then the mobile APP can play different music according to different values in the XML file. Our APP interface is shown in Fig. 2.

III. Breathing Rate Estimation

By extracting the CSI data matrix, as shown in Fig. 3, the CSI of the pth packet collected at each moment can be arranged as a three-dimensional data $(n \times m \times k)$, and the sampling value of the CFR on the kth subcarrier between the nth transmit antenna and the mth receive antenna is denoted as $H_{n,m,k,p} = |H_{n,m,k,p}|e^{j\theta_{n,m,k,p}}$, where $|H_{n,m,k,p}|$ and $\theta_{n,m,k,p}$ represent the amplitude and phase of an OFDM subcarrier, respectively.

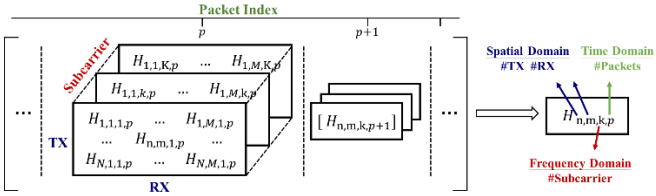

Fig. 3 The CSI data matrix

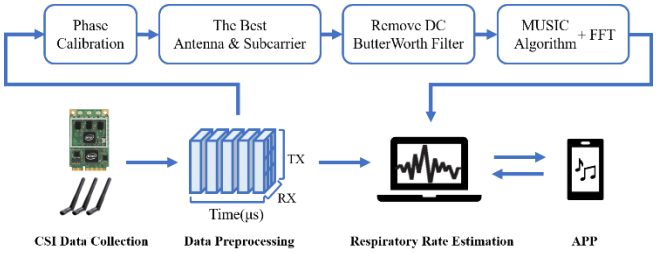

Fig. 4 The flow chart of the breathing rate estimation.

Fig. 4 shows the flow chart of the breathing rate estimation, and the procedures are elaborated as follows. In addition to the common phase of the wireless channels, the estimated CSI phase is also affected by the different phase rotation of delay on subcarriers, the random phase offset, and random noise, and it can be modeled as [2]:

$$\theta_{n,m,k,p} = \breve{\theta}_{n,m,k,p} + \frac{2\pi I_k \Delta t}{N} + \beta_{n,m,k,P} + z_{n,m,k,p}\,, \quad (1)$$

where $\check{\theta}_{n,m,k,p}$ represents the real phase, Δt is the delay error, $\beta_{n,m,k,P}$ is the random phase offset caused by the device, $z_{n,m,k,p}$ is the random noise during the measurement, I_k is the subcarrier index (in IEEE 802.11n, the range is [-28, 28]). Let K be the total number of CSI subcarriers. Therefore, the estimation of real phase $\check{\theta}_{n,m,k,p}$ can be refined as [2]:

$$\hat{\theta}_{n,m,k,p} = \theta_{n,m,k,p} - \frac{\theta_{n,m,k,p}-\theta_{n,m,1,p}}{I_n - I_1} I_k - \frac{\sum_{k=1}^{K} \theta_{n,mk,p}}{K}, \quad (2)$$

where the second term on the right-hand side is the estimation of the phase rotation caused by the delay error to get the real CSI phase, while the third term is the estimation of $\beta_{n,m,k,P}$.

In order to filter out those CSIs on the antennas and subcarriers which are not significantly changed in each packet, the CSI amplitude variation $\sigma_{n,m,k}^2$ is used to quantify its sensitivity to the breathing state. We first calculate the CSI amplitude variation $\sigma_{n,m}^2$ of the sum of the subcarriers in each antenna path. The calculation method is as follows

$$\sigma_{n,m}^2 = \sum_{p=1}^{P} |H_{n,m,p}|^2 - (\sum_{p=1}^{P} |H_{n,m,p}|)^2 \quad ; \quad (3)$$

$$(\tilde{n}, \tilde{m}) = \arg \max_{n=1..3, m=1..3} (\sigma_{n,m}^2) \ , \quad (4)$$

where

$$|H_{n,m,p}| = \sum_{k=1}^{K} |H_{n,m,k,p}| \quad . \quad (5)$$

After selecting the antenna path $(\tilde{n}, \tilde{m})$ in Fig. 5, there are thirty subcarriers on the selected antenna pair which is shown in Fig. 6. We then choose the best subcarrier by calculating the CSI amplitude variation $\sigma_{\tilde{n},\tilde{m},k}^2$, and the calculation method is as follows:

$$\sigma_{\tilde{n},\tilde{m},k}^2 = \frac{1}{P-1} \sum_{p=1}^{P} \left[|H_{\tilde{n},\tilde{m},k,p}| - \sum_{p=1}^{P} (|H_{\tilde{n},\tilde{m},k,p}|) \right]^2 \quad (6)$$

$$\tilde{k} = \arg \max_{k=1...30} (\sigma_{\tilde{n},\tilde{m},k}^2) \quad (7)$$

$$\tilde{\theta}_p = \hat{\theta}_{\tilde{n},\tilde{m},\tilde{k},p} \quad (8)$$

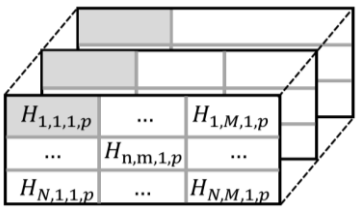

Fig. 5 The CSI data on the selected antenna pair.

Fig. 6 After selecting the best antenna pair $(\tilde{n}, \tilde{m})$, select the collected CSI packets on the best subcarrier $\tilde{k}$.

Now, $\tilde{\theta}_p$ is the estimation of the real phase after selecting the best antenna pair and subcarrier. Then we remove the DC component from the signal $\tilde{\theta}_p$ and set the cut-off frequency of the band-pass Butterworth filter at 0.16Hz ~ 0.6Hz to filter out the rest of the unnecessary noise parts.

We use the MUSIC algorithm for frequency estimation. It is a method based on matrix eigenspace decomposition, which decomposes the observation space of signals into a signal subspace and a noise subspace. We arrange the one-dimensional signal $\tilde{\boldsymbol{\theta}} = [\tilde{\theta}_1, \tilde{\theta}_2, \ldots, \tilde{\theta}_P]$ in stepwise to form a matrix $\boldsymbol{Q}$ of $(P - X + 1) \times X$ after executing the band-pass filter processing, and $\tilde{q}_{i,l}$ is an element of the matrix $\boldsymbol{Q}$:

$$\boldsymbol{Q} = \begin{bmatrix} \tilde{q}_{1,1} & 0 & 0 & 0 \\ \tilde{q}_{2,1} & \tilde{q}_{1,2} & 0 & 0 \\ \vdots & \tilde{q}_{2,2} & \ddots & 0 \\ \vdots & \vdots & \ddots & \tilde{q}_{1,X} \\ \vdots & \vdots & \ddots & \vdots \\ \tilde{q}_{P,1} & \vdots & \ddots & \tilde{q}_{(P-X+1),X} \\ 0 & \tilde{q}_{P,2} & \ddots & \vdots \\ 0 & 0 & 0 & \tilde{q}_{P,X} \end{bmatrix} . \quad (9)$$

Then we use the matrix $\boldsymbol{Q}$ to generate a covariance matrix $\boldsymbol{R}$ that can generate a signal of length P into X sample spaces:

$$\boldsymbol{R} = \frac{1}{X-1} \boldsymbol{Q}^H \boldsymbol{Q} \quad . \quad (10)$$

By decomposing the covariance matrix $\boldsymbol{R}$ into eigenvalues and eigenvectors, we can get $\boldsymbol{RV} = \boldsymbol{DV}$, where $\boldsymbol{D}$ is the eigenvalue matrix and $\boldsymbol{V}$ is the eigenvector matrix. By sorting the eigenvalues in an ascending order, the signal subspace is composed of the eigenvector matrices with the E largest eigenvalues. On the contrary, the noise subspace is composed of the remaining $X - E$ eigenvector matrices. The two subspaces are mutually orthogonal spaces. We let $\boldsymbol{V} = [\boldsymbol{v}_1, \boldsymbol{v}_2, \ldots, \boldsymbol{v}_{X-E}]$ be the eigenvector matrix of the noise subspace. Denote the vector $\hat{\boldsymbol{v}}_i$ as the frequency-domain representation of the vector $\boldsymbol{v}_i$, which can be obtained by taking the N-point fast Fourier transform (FFT) operation. Afterwards, $X - E$ vectors $\hat{\boldsymbol{v}}_i$ are added to get $\boldsymbol{b} = \sum_{i=1}^{X-E} \hat{\boldsymbol{v}}_i = [b_1, b_2, \ldots, b_N]$, and then we search for the discrete frequency position with the largest reciprocal value of b_j:

$$\hat{j} = arg \max_{j=1,\ldots,N} \frac{1}{b_j} \quad ; \quad (11)$$

$$F_{\hat{j}} = (\hat{j} - 1) \times \frac{F_s}{N} \quad , \quad (12)$$

where F_s is the sampling frequency. Here, we set the sampling frequency to 10 Hz so that there would be enough sampling points for FFT in each minute. As a result, $F_{\hat{j}}$ is the estimated breathing rate.

IV. Experiment Results and Discussions

A. Observe the phase change of CSIs and calculate the breathing rate

Fig. 7 shows the proposed breathing rate monitoring system and the experimental scenario. In this experiment, the breathing rate of a subject is 24 bpm via conventionally

counting. The CSI phase change and the breathing rate estimation can be observed in Fig. 8. In Fig.8(a), there are 24 obvious peaks, and the number of peaks is the same as the number of the subject's breathing rate. In Fig.8(b), it demonstrates that the result calculated by the MUSIC algorithm has the highest peak at around 0.4Hz, which is equivalent to 24 bpm. Therefore, the estimation of the breathing rate can be successfully figured out not only from the number of peaks of the de-noised CSI phase change but also via the MUSIC.

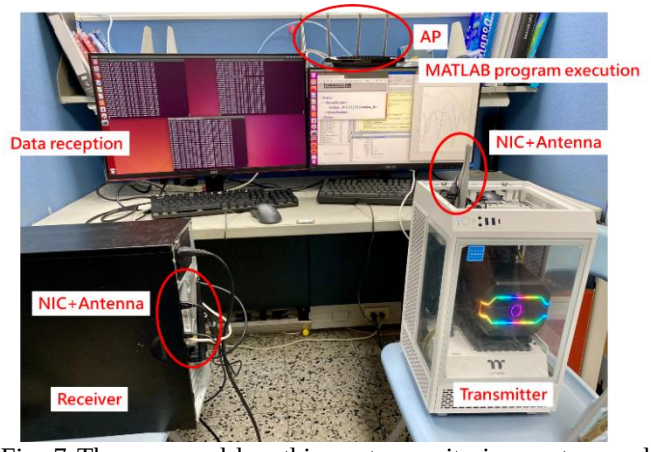

Fig. 7 The proposed breathing rate monitoring system and experimental scenario

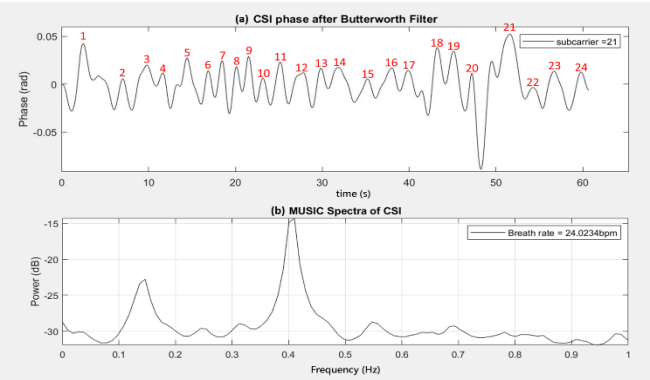

Fig. 8 The subject's CSI phase change and breathing rate estimation.

B. *Different breathing rates at different moment*

In this experiment, the subject alters his breathing states, including fast, slow, and apnea, as listed in Table 1. In Fig. 9, it shows that when the breathing rate is fast, there are more peaks in the observation period; when the breathing rate is slow, the number of peaks becomes less. However, when the breathing state is apnea, the CSI phase changes relatively smooth during the period, and there are no obvious peaks and valleys which are different from the situations of inhalation and exhalation.

Ultimately, since the breathing state includes fast, slow and apnea at the same time, the relatively accurate breathing rate cannot be estimated. If the number of the largest eigenvalue is set too small, the frequency estimation cannot be done correctly in the MUSIC algorithm. On the other hand, if the number is set too large, it may impose some unnecessary noise in the breathing rate calculation, yielding the frequency estimation error.

Time	State	Number of peaks	Frequency
0~30s	Fast	15	0.5
30~40s	Apnea		
40~60s	Slow	7	0.35
60~70s	Apnea		
70~90s	Fast	10	0.5
90~100s	Apnea		
100~120s	Slow	8	0.4

Table 1 Experimental value of breathing rates at different time.

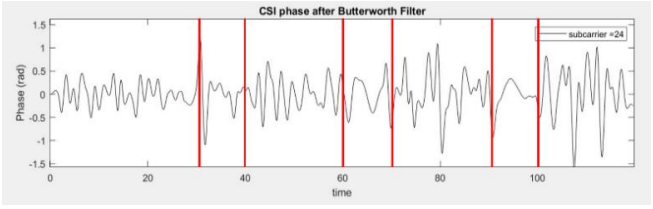

Fig. 9 CSI phase changes at different moment.

C. *The detection of apnea state*

In this experiment, we try to observe the apnea state. In a minute, the subject takes a big breath at the beginning of every ten seconds, then hold his breath until the beginning of the next ten seconds. In Fig. 10, we can find that there are obvious peaks when a strong inhalation occurs. By contrast, there are no large fluctuations during the apnea, and the trend reflected by the CSI phase is relatively smooth. There are six obvious peaks in total according to Fig. 10, and thus, if we estimate the breathing rate by counting the number of peaks during the observation period, the result also matches.

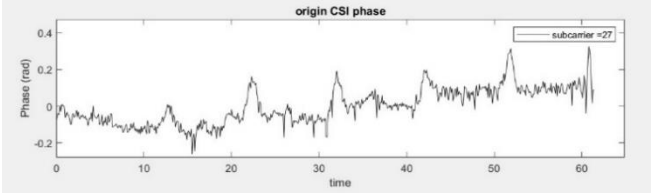

Fig. 10 CSI phase change in apnea.

D. *One person changing the breathing rate in a period*

In Fig. 11 and Fig. 12, we demonstrate an experiment where there is only one person and he has two kinds of breathing rates in one minute. We can find that the sudden change of the breathing rate, which changes the exercise of the chest cavity, also affects the CSI in the channel environment. Hence, the experiment result shows two trends of the linear transformation of the CSI phases in Fig. 11. According to Fig. 12, it shows that the proposed system can also distinguish two kinds of breathing rates.

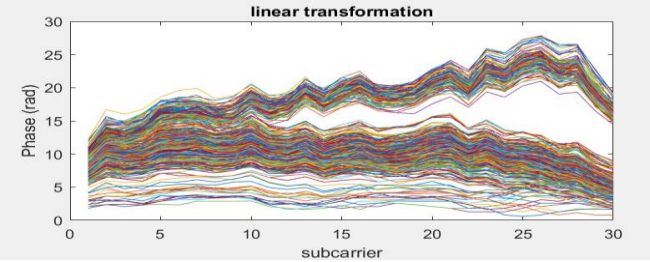

Fig. 11 CSI phase linear transformation diagram of the breathing rate change.

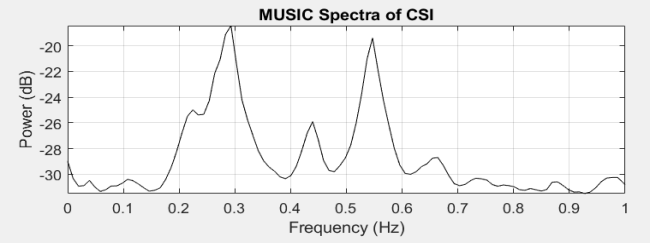

Fig. 12 Breathing rate estimation for the breathing rate changes.

E. Two people breathing at the same time, with different fixed breathing rates

In this experiment, there are two people with different breathing states but maintain fixed breathing rates for one minute. The breathing rates of the two people are 41 and 10 bpm, respectively. Since the breathing rates are unchanged during the observation period, the CSI in the channel environment is relatively stable. Hence, only one trend of the linear transformation of the CSI phases is observed in Fig. 13 Besides, Fig. 14 shows that the proposed system can truly distinguish the breathing rates of two people.

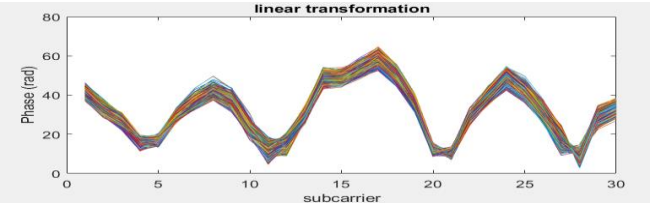

Fig. 13 The CSI phase linear transformation of two people.

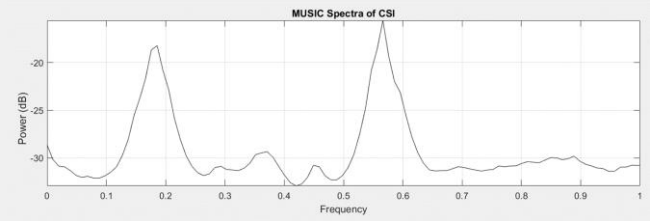

Fig. 14 Breathing rate estimation for two people.

V. Conclusions

In this paper, we propose a MUSIC-based breathing rate monitoring system using Wi-Fi CSIs. The antenna and subcarrier selection mechanisms are designed to select those CSIs that are sensitive to breathing changes. In addition, the MUSIC algorithm is applied to effectively extract the breathing rates. Throughout the experiments, we find that in general situations, the proposed breathing monitoring system can successfully distinguish fast breathing, slow breathing, and hold-breathing states. It is worth mentioning that there are not many devices on the market that can effectively detect breathing rates, and most of them are wearable wristbands with high unit prices. Based on our experiment validation, it is a promising solution to apply the CSIs to the breathing rate estimation or monitoring of physiological information.

Acknowledgement

This work was supported by the Ministry of Science and Technology of Taiwan, under Grant MOST 111-2221-E-008-042-MY3 and National Science and Technology Council, Taiwan, under Grant 111-2813-C-008-024-E. The work of Chih-Min Yu was supported in part by the Natural Science Foundation of Fujian Province, China, under Grant 2020J01089.

References

[1] https://github.com/spanev/linux-80211n-csitool
[2] X. Wang, C. Yang, and S. Mao, "PhaseBeat: Exploiting CSI Phase Data for Vital Sign Monitoring with Commodity WiFi Devices," in Proc. *IEEE ICDCS*, pp. 1230-1239, 2017.
[3] H. Abdelnasser and M. Youssef, "UbiBreathe: A Ubiquitous non-Invasive WiFi-based Breathing Estimator," in Proc. *ACM MobiHoc*, pp. 277-286, 2015.
[4] J. Liu, Y. Wang, Y. Chen, J. Yang, X. Chen, and J. Cheng, "Tracking Vital Signs During Sleep Leveraging Off-the-self WiFi," in Proc. *ACM MobiHoc*, pp. 267-276, 2015.
[5] Y. Gu, X. Zhang, Z. Liu, and F. Ren, "WiFi-based Real-time Breathing and Heart Rate Monitoring during Sleep," in Proc. *IEEE GLOBECOM*, pp.1-6,2019.
[6] H. Wang, D. Zhang, J. Ma, Y. Wang, Y. Wang, D. Wu, T. Gu, and B. Xie, "Human Respiration Detection with Commodity WiFi Devices: Do User Location and Body Orientation Matter?" in Proc. *ACM UbiComp*, pp. 25–36, 2016.
[7] E. O. Brigham and R. E. Morrow, "The Fast Fourier Transform," *IEEE Spectrum*, vol. 4, no. 12, pp. 63-70, Dec. 1967.
[8] Y. Liu and F. Gao, "Research of Multiple Signal Classification in Massive MIMO Systems," in Proc. *IEEE ITNEC*, pp. 1205-1208, 2017.